# Preparation of Interfacially Compatibilized PP-EPDM Thermoplastic Vulcanizate/Graphite Nanocomposites: Effects of Graphite Microstructure upon Morphology, Electrical Conductivity, and Melt Rheology

**A. A. Katbab,[1] A. N. Hrymak,[2] K. Kasmadjian[2]**

[1]*Department of Polymer Engineering, Amirkabir University, Tehran, Iran*
[2]*Department of Chemical Engineering, Mcmaster University, Hamilton, Ontario, L8S4L 7, Canada*

Received 8 May 2007; accepted 22 August 2007
DOI 10.1002/app.27454
Published online 3 December 2007 in Wiley InterScience (www.interscience.wiley.com).

**ABSTRACT:** Electrically conductive PP/EPDM dynamically crosslinked thermoplastic vulcanizate (TPV)/expanded graphite (EG) has been successfully prepared via melt compounding of maleic anhydride grafted polypropylene (PP-*g*-MA)/EG masterbatch and a commercially available TPV material. Correlation between graphite microstructure, and electrical conductivity as well as melt rheological behavior has been studied. Natural graphite flake (NGF), graphite intercalated compound (GIC), and exfoliated graphite (EG) have been employed and compared. Scanning electron microscopy (SEM) showed the presence of 100–200 nm nanolayers in the structure of PP-*g*/EG masterbatches, whereas thinner platelets (1.5–2.5 nm) were revealed by transmission electron microscopy (TEM). Better dispersion of the graphite nanolayers in the microstructure of TPV/PP-*g*-MA/EG composite was verified, as the 7.3 Å spacing between the aggregated graphite nanolayers could not be observed in the XRD pattern of this material. TPV/PP-*g*/EG nanocomposites exhibited much lower conductivity percolation threshold ($\varphi_c$) with increased conductivity to $10^{-5}$ S/cm at EG wt % of 10. Higher nonlinear and nonterminal melt rheological characteristics of dynamic elastic modulus ($G'$) at low frequency region was presented by the TPV/PP-*g*/EG nanocomposites, indicating the formation of nanoscopic conducting multiple networks throughout the continuous TPV matrix. Maleated PP was found to be much more effective in separating EG nanolayers which is attributed to the higher interfacial interaction between PP-*g*-MAH and EG, synergized with its multiporous structure. © 2007 Wiley Periodicals, Inc. J Appl Polym Sci 107: 3425–3433, 2008

**Key words:** PP; EPDM; thermoplastic vulcanizate; conductivity; nanocomposite; morphology; expanded graphite (EG)

## INRODUCTION

Polymer nanocomposites have been known as new and potential class of materials alternative to conventional-filled polymers (microcomposites). This is because of markedly improved and enhanced properties coupled with lightweight, which are attributed to the nanoscale dispersion of the nanoscopic filler throughout the polymer matrix, which makes the reinforcement possible at a very low loading of the nanofiller compared with the conventional fillers.[1–5] The most often used nanofillers are clay, alumina, gold, silver, nano tubes, and graphite.[6,7] Unfortunately, nanoclay reinforced polymers do not possess any significant electrical conductivity, photonic, and magnetic properties compared with other functional polymer composites based on carbon black, carbon fiber, graphite, and carbon nanotubes.

Conducting polymer composites have attracted great attention and are the high light in interference shielding and antistatic materials as well as pressure sensors.[8–11] The most widely used conducting fillers are metal powders, carbon black, graphite, carbon fiber, etc.[12–16] The conductivity of the polymer composites based on these fillers is mainly varied as a function of the filler content, and explained by the percolation theory.[17,18] When the filler level reaches a critical value which is called percolation threshold, sharp transition from insulator to conductor is observed with slight increase of the filler content. However, high filler level is needed to reach the critical value which results in poor processability and diverse effects upon the mechanical properties.

Like layered silicates, natural flake graphite is composed of nanosheets with the spacing of 0.66 nm, and is a good electrical conductor with conductivity of $10^{+4}$ S/cm at room temperature.[18–20] The carbon layers are bound by weak van der waals forces which allows the intercalation of small molecules in between the carbon layers. The resulting products are called graphite intercalating compound (GIC).[21] However, unlike nanoclay whose intercalation can be achieved by ion exchange reaction into the galleries, intercalation of graphite can not be done by

*Correspondence to:* A. A. Katbab (katbab@aut.ac.ir).

Journal of Applied Polymer Science, Vol. 107, 3425–3433 (2008)

**TABLE I**
**Physical Characteristics of the used Materials**

| Material | Hardness (shore A) | Density ($g/cm^3$) | Physical form |
|---|---|---|---|
| Santoprene (261-87) | 87 | 0.97, at 23°C | White off pellets |
| PP-*g*-MA polybond 3200 | – | 0.93, at 20°C | White off pellets |

the same way. Therefore, exfoliation of the graphite nanolayers is carried out by subjecting the GIC to a sudden thermal shock at a very high temperature (> 900°C), which results in a high expansion of the graphite layers in *c*-axis direction, called expanded graphite (EG). EG has a worm-like vermicular porous structure with pores ranging from 10 nm to 10 μm.[22] Recently, thermoplastic/EG electrically conductive nanocomposites have attracted great attention, as a very low volume fraction is needed to reach the percolation threshold, and electrical conductivity of the polymer can be increased to $10^{-4}$ S/cm with a very low EG content. In the past few years, conductive thermoplastic nanocomposites based on EG have been mostly fabricated by monomer intercalation, *in situ* polymerization,[23–25] and solution intercalation.[26,27] However, melt mixing preparation of electrically conductive thermoplastic/EG nanocomposites have become important as it is preferred for many industrial applications.[28]

Dynamically vulcanized thermoplastic elastomers or thermoplastic vulcanizates (TPVs) specially those based on polyolefins (PP, PE), and EPDM rubber have been widely used for various electrical purposes as they can be melt-processed similar to the conventional thermoplastics, but having rubbery characteristics at low temperatures.[29,30] However, no work has so far been reported on TPV/graphite nanocomposites.

The object of the present work was to prepare nanocomposite thermoplastic vulcanizates (N-$TPV_s$) by dispersing graphite nanolayers throughout the TPV matrix via melt mixing process. The effect of the initial graphite microstructure and interfacial compatibilization upon the developed microstructure of the TPV/graphite composite have been investigated. Correlation between the TPV/graphite composite morphology and conductivity percolation threshold as well as the melt rheological behavior has also been studied.

## EXPERIMENTAL

### Materials

The graphites used in this work were natural flaky graphite (NGF) with an average diameter of 3–5 μm and surface area of 13 $m^2/g$, expandable or GIC with an average size of 20 × 50 $\mu m^2$ and volume expansion ratio of 300. Both graphites were used as received, and supplied from Asbüry carbons (USA) by the commercial name of Micro 850 and 772, respectively. Expanded or exfoliated graphite was prepared by subjecting the GIC graphite to a sudden thermal shock at 950°C for 15 s in a furnace. At such a condition, the intercalated graphite showed rapid exfoliation of its nanolayers with enormous increase in volume and expansion of about 50–100 times in the thickness or *c*-direction. The EG emerged as a loose and multiporouse material with pores in the range of 10–100 μm, and consisting of nanolayers with the thickness of 100–400 nm. The surface area of the EG has been reported to be roughly 30–40 $m^2/g$ and pore volume of 4–8 mL $g^{-1}$.[28] The PP-*g*-MA with the trade name polybond 3200, having graft ratio of 0.9–1 wt % and a melt index of 110 g/10 min was used as compatibilizer and supplied by Crompton—Uniroyal Chemical. TPV was commercially available as santoprene TPV 261-87 supplied by Advanced Elastomers Systems, L.p, and comprising dynamically crosslinked EPDM rubber dispersed in the polypropylene matrix. The physical characteristics of TPV and PP-*g*-MA are given in Table I.

### Melt compounding and sample preparation

To prepare TPV/PP-*g*-MA/graphite compounds, PP-*g*-MA was first master batched separately with each graphite material via melt mixing process in a laboratory size internal mixer model thermo Haake polylab system with the chamber volume of 300 $cm^3$, at 190°C and mixing speed of 25 rpm for 15 min. All materials were predried in a vacuum oven at 60°C prior to mixing, and solid density of EG was taken as 2.26 $g/cm^3$.[31] In all masterbatches, the weight fraction of PP-*g*-MA to graphite was kept constant ($f_w$ = 3). Prepared masterbatches were ground into powder, and then mixed with santoprene TPV in a separate melt mixing process at 200°C and 25 rmp for 20 min. Various TPV/masterbatch compounds containing different weight fractions of graphite were prepared. The mixing was carried out by first feeding the TPV into the mixer and after 2 min the masterbatch powder was added in two stages. The prepared TPV/masterbatch compounds were ground into powder and then compression moulded into sheets with 0.5 mm thickness in a hot press at 190°C for 2 min. The masterbatch compounds which were synthesized, compositions of their corresponding TPV/PP-*g*-MA/graphite composites have been described in Tables II and III, respectively.

### Electrical conductivity measurements

Volume conductivity (σ) of different predried samples was evaluated at room temperature by a stand-

**TABLE II**
**Prepared Masterbatch Compounds with the *g*-PP to Graphite Fraction Ratio ($f_w$) of 3**

| Master batch | PP-*g*-MA (wt %) | Graphite (wt %) | | |
|---|---|---|---|---|
| | | NGF | GIC | EG |
| MN | 150 | 50 | – | – |
| MGIC | 150 | – | 50 | – |
| ME | 150 | – | – | 50 |

ard four-probe points digital multimeter model Agitent-E 3641A equipped with a DC voltage/current generator. The hot pressed flat rectangle sheet samples were cut into specimens of $10 \times 4 \times 0.5$ mm$^3$ for conductivity tests. Silver paste was used to assure good contact of the sample surfaces with the electrodes. The conductivity data were read at 1 s after applying the voltage.

### Microstructure characterization

#### X-ray diffractometery

The structure of graphite materials, and their corresponding composites were determined by performing X-ray diffractometery (XRD) analysis using a Bruker D8 Advanced diffractometer (Cu K, radiation), $\lambda = 1.54$ Å, generator voltage of 40 kv, and current 40 μA. Samples were radially scanned at room temperature within the angle range of $2\theta = 2^\circ$–$4^\circ$, and scanning rate of $0.1^\circ$/min.

#### Transmission electron microscopy

A transmission electron microscopy (TEM) model JEOL 1200 EX was employed to evaluate the degree of separation and dispersion of the graphite nanolayers onto the polymer matrix. Ultrathin sections with a thickness of ≈ 100 nm were obtained by microtoming the frozen plates using an ultrahigh microtome.

#### Scanning electron microscopy

The microstructure of different graphite powders and their degree of dispersion in both PP-*g*-MA and corresponding TPV/masterbatch compounds were visualized with scanning electron microscopy (SEM) model Philips 515. The plate type polymer samples were cryo fractured and then gold sputtered under vacuum.

#### Melt viscoelastic studies

Melt rheology and viscoelastic behavior of the samples were measured using a parallel plate rheometer model ARES (Canada) with thermo chamber model ARES. For this purpose, disk samples with 2.5 mm in diameter and 1.8–2 mm thickness were used, and rheometer was operated at 220°C in dynamic mode with parallel-plate fixture and gap distance of 1.5 mm. Strain sweep was first performed on each sample in the range of 0.1–100% in order to determine the linear viscoelastic region, and then frequency sweep was carried out on the same sample within the linear regime between 0.01 and 100 $s^{-1}$ shear rate to evaluate the frequency dependency of the melt viscosity as well as dynamic storage modulus ($G'$).

## RESULTS AND DISCUSSION

### Structural analysis

Natural graphite is in the form of flakes that are composed of graphite layers with the thickness of less than 100 nm.[22] The layers are further aggregates of parallel sheets with 1–2 nm in the thickness. The aggregates have been reported to be separated by a gallery spacing of 7–16 Å,[26] and contain carbon layers stacked on top of each other by weak van der waals forces with the spacing of 3.35 Å. The weak interplanar forces allow intercalation of natural graphite by small molecules. The chemically modified graphite known as GIC, is composed of intercalated layers stacked in a periodic fashion.[26] When GIC was subjected to a sudden high temperature (≈ 950°C), it expanded up to several hundred of times along the *c*-axis of graphite, forming a worm-like multiporous structure composed of parallel lamellae with the thickness ranging from 100 to 600 nm as illustrated in Figure 1(b,c). However, magnified SEM micrograph of EG [Fig. 1(d)] revealed thinner layers in the structure of the used EG. XRD patterns of three graphite samples are presented and compared in Figure 2. It is clearly observed that NGF exhibits, a sharp and narrow peak at $2\theta = 26.5^\circ$, and a broad peak with it's maxima at $2\theta = 13^\circ$, corresponding to the spacing of 3.5 and 7.3 Å, respectively. However, GIC spectrum shows an intense but wider peak at $2\theta = 20$–$35^\circ$, indicating increased interplanar spacing between the nano-

**TABLE III**
**Compositions of Prepared TPV/PP-*g*-MA/Graphite Composites**

| Composites | Components | |
|---|---|---|
| | Master batch | TPV |
| NC-MN-X[a] | MN | Santoprene-261-87 |
| NC-MGIC-X | MGIC | Santoprene-261-87 |
| NC-ME-X | ME | Santoprene-261-87 |
| NC-TPV-EG[b] | – | Santoprene-261-87 |

[a] *X*, denotes masterbatch wt % (2, 4, 6, 8, 12, 24, 32, 40).
[b] Composites prepared by direct melt mixing of TPV with EG (0.5, 1, 1.5, 2, 3, 6, 8, and 10 wt %).

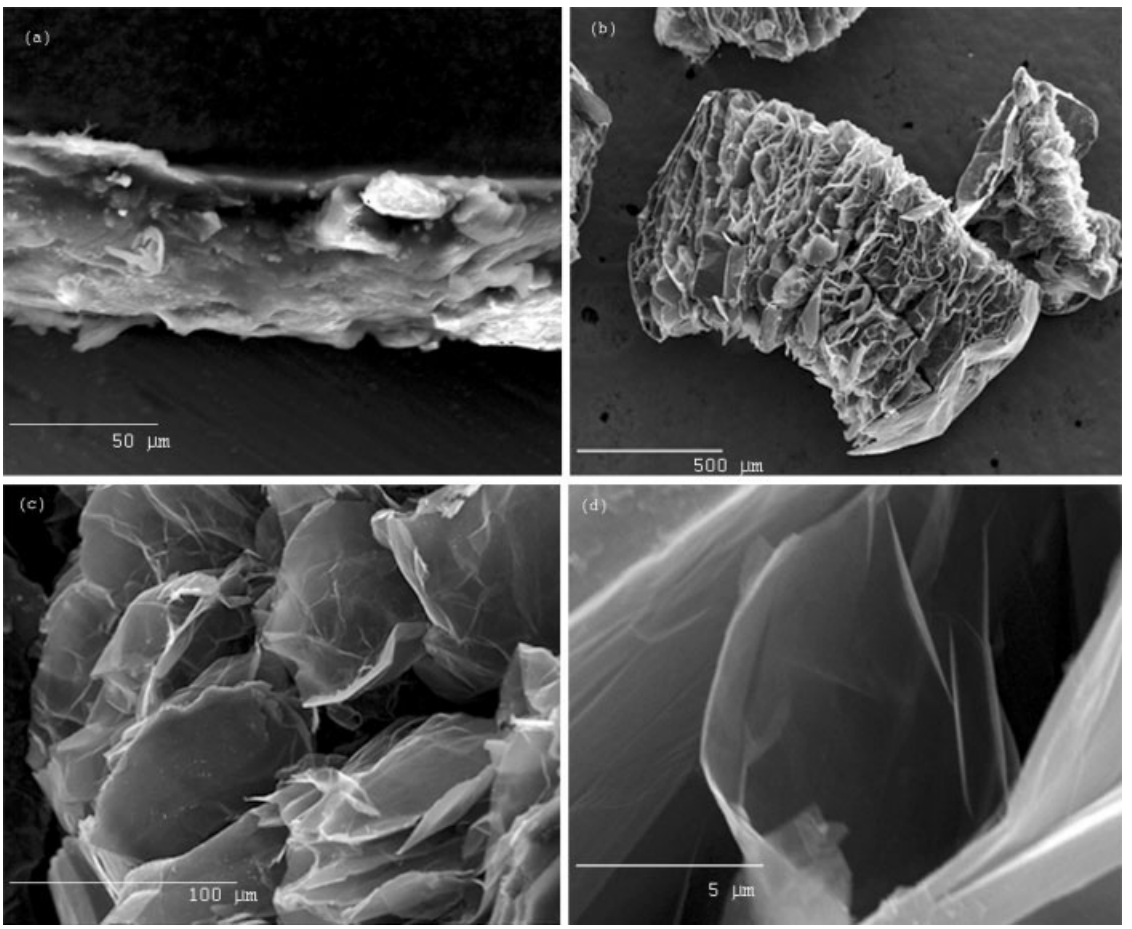


**Figure 1** SEM photomicrographs of, (a) graphite intercalated (GIC), (b–d) expanded graphite at different magnifications.

layers and also existence of different intercalation stages in the structure of the used GIC.[32] The XRD diffraction pattern of EG exhibits also a wide and intense peak within the range of $2\theta = 23–30^{\circ}$, but more uniform spacing between its exfoliated nanolayers compared with GIC.

To obtain more understanding of the molecular interaction between the *g*-PP and graphites with different structure, and also the morphology developed as a result of melt compounding, electron microscopy (SEM, TEM) and XRD were conducted on the samples of the prepared masterbatches. Figure 3 shows SEM photomicrographs of the masterbatch composites based on NGF, GIC, EG, denoted as MN, MGIC, ME, respectively. It is clearly observed in Figure 3(a) that the original structure of the natural graphite has been retained with the unfolded nanolayers stacked parallel to each other has been retained and not affected by the applied shear during mixing process with *g*-pp. SEM image of the MGIC [Fig. 3(b)] indicates a multiporous structure for the graphite phase in which deformed and folded nanolayers are separated as a result of high-pressure build-up during compounding. However, SEM micrograph of ME [Fig. 3(c)] clearly demonstrates the dispersion of the graphite platelets parallel to each other with good interconnectivity. TEM examination was performed on ultrathin samples of ME, as illustrated in Figure 4. The black lines and white domains in the TEM image are denoted to the exfoliated EG nanosheets and PP-*g*-MA matrix,

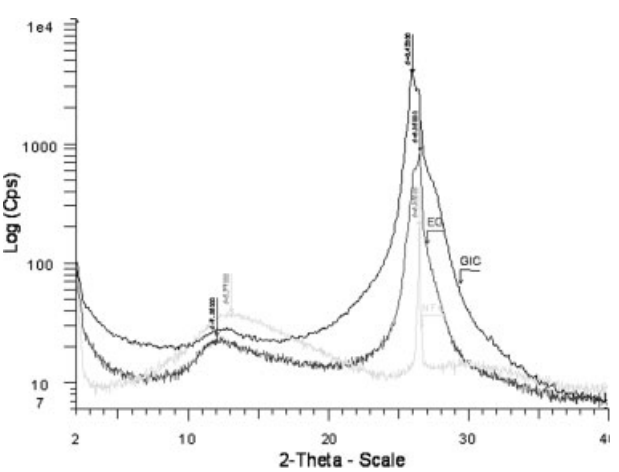


**Figure 2** XRD patterns of natural flake graphite (NFG), graphite intercalated compound (GIC), and expanded graphite (EG).

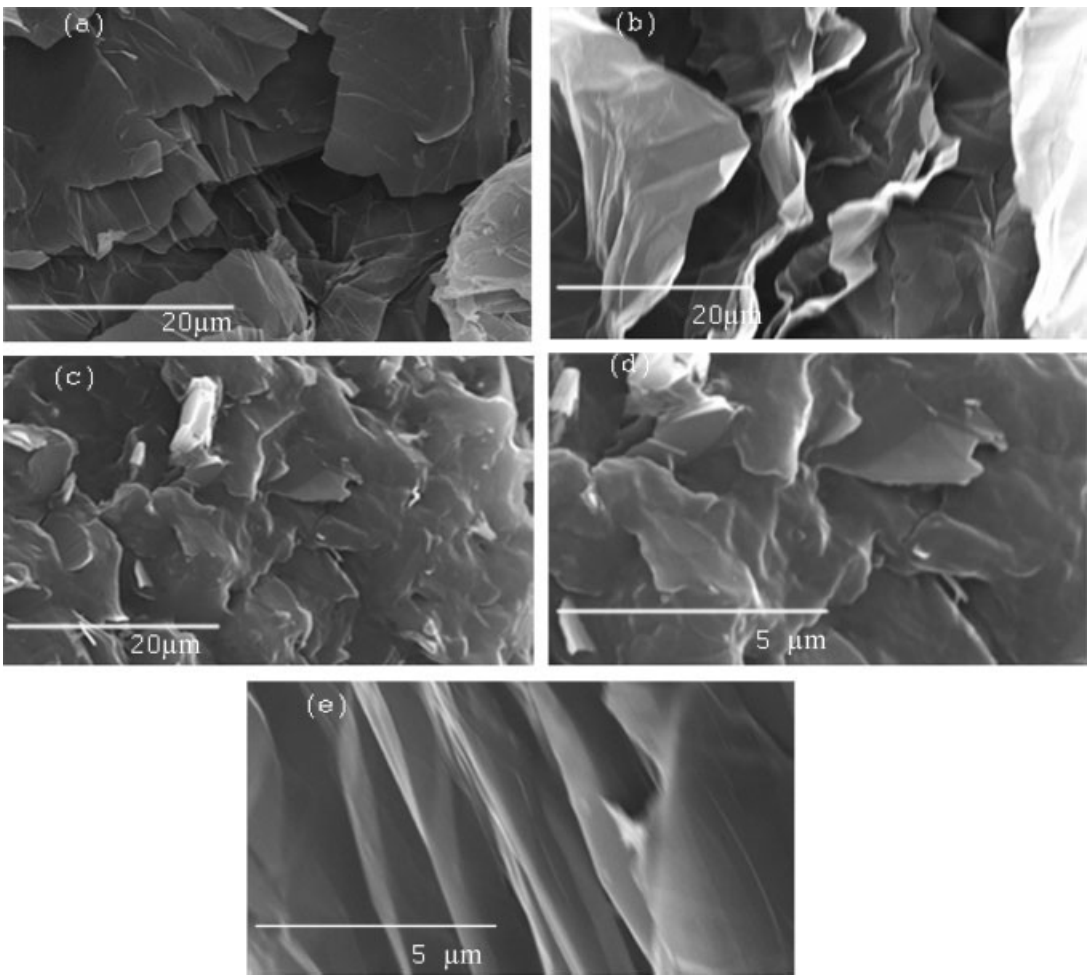


**Figure 3** SEM photomicrographs of masterbatches based on PP-*g*-MAH, (a) NGF, (b) GIC, (c–e) EG, denoted as MN, MGIC, ME, respectively.

respectively. The nanosheets have appeared with high aspect ratio (length to thickness) and average spacing of 45 Å.

Comparing the XRD patterns of MN and ME [Fig. 5 (a)] leads to the conclusion, that molten PP-*g*-MA chains have preferentially been adsorbed onto the micron size pores in the structure of EG, as interplanar spacing peak at 7.2 Å has not been eliminated in the XRD patterns of both MN and ME. Interestingly, this peak has been removed in the XRD spectrum of MGIC as a result of pressure induced separation of GIC nanolayers during mixing which permits intercalation of the PP-*g*-MA molecules and consequently significant isolation between the GIC nanolayers.

Figure 6 plots the XRD pattern of the nanocomposite material prepared by melt mixing of TPV with 12 weight percent of ME masterbatch. It is observed in this Figure that the interplanar diffraction peak at the diffraction angle of 12.5 (2θ) corresponding to the 7.2-Å spacing between the graphite nanolayers has been eliminated, indicating that EG nanolayers

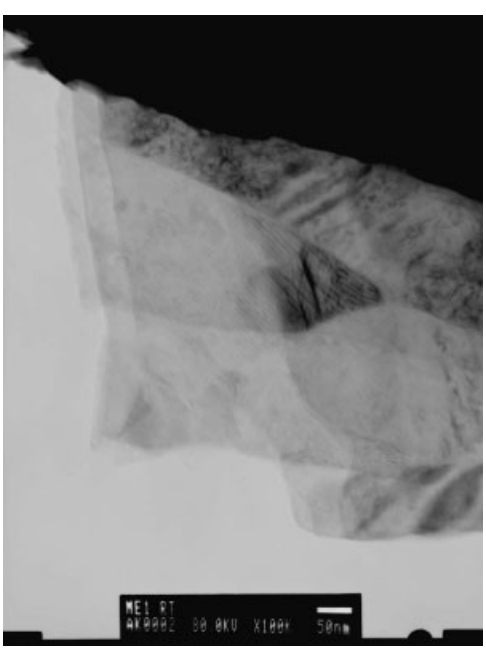

**Figure 4** TEM micrograph of PP-*g*-MA/EG masterbatch sample.

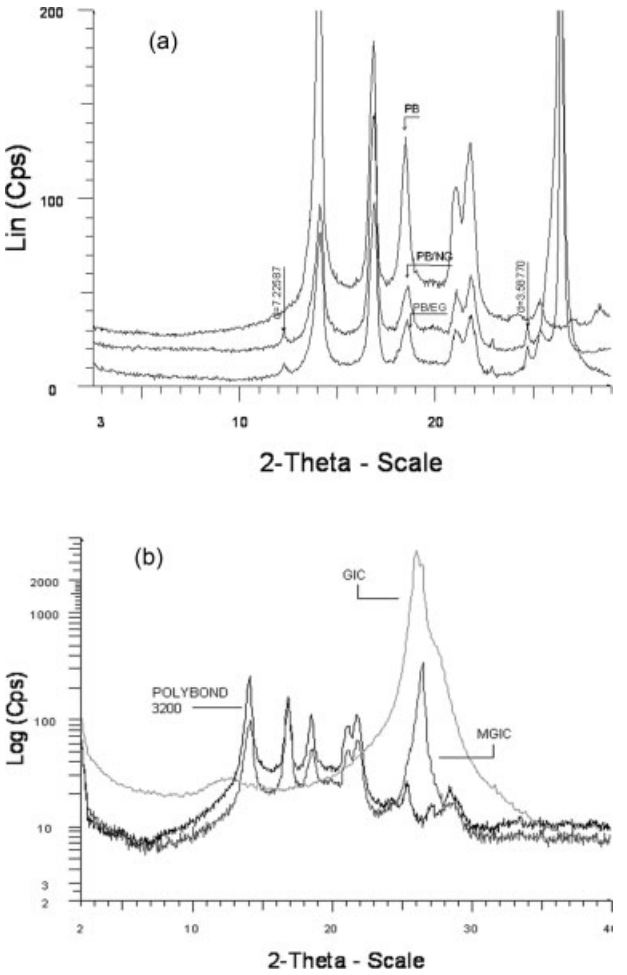


**Figure 5** XRD patterns of the prepared masterbatches based on polybond 3200 and, (a) natural graphite (NFG) and expanded graphite (EG), (b) PP-*g*-graphite intercalated (GIC).

have almost been delaminated as a result of intensive shear mixing exerted by the highly viscous molten TPV during mixing process. However, no significant expansion has occurred to the gallery spaces of the graphite carbon nanolayers ($2\theta = 26.5^\circ$), implying that TPV chains have not been able to diffuse into the galleries of carbon layers. This is also consistent with the SEM image of the TPV/pp-*g*-MA/EG nanocomposite as illustrated in Figure 7. It is clearly seen in the magnified SEM micrograph [Fig. 7(b)] that graphite nanosheets with the thickness of 30–60 nm exist in the matrix of this composite. Based on these results, the mechanism by which the morphology and nanostructure is developed by melt mixing of EG with pp-*g*-MA and subsequent mixing of the obtained masterbatch with the TPV material could be modeled as illustrated in Figure 8.

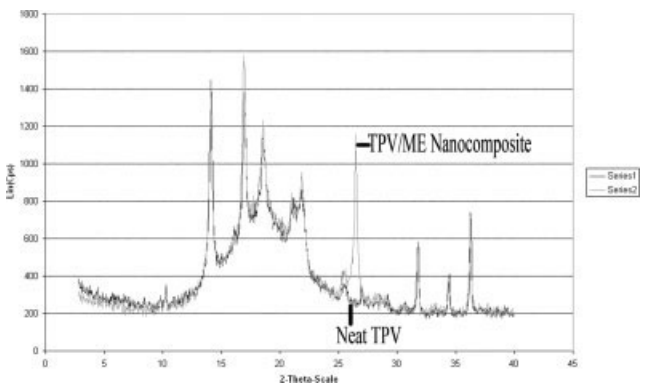


**Figure 6** Comparison between XRD patterns of the neat santoprene TPV(1), and TPV nanocomposite composed of 12 wt % of ME (3 wt % EG).

## Melt rheological properties

Melt rheological characterization has been found as an informative and complimentary method to XRD and electron microscopic techniques (SEM, TEM) to reveal better understanding of the nanofiller dispersion state in the hybrid polymer nanocomposites.[32,33] The melt viscoelastic behavior of nanocomposites

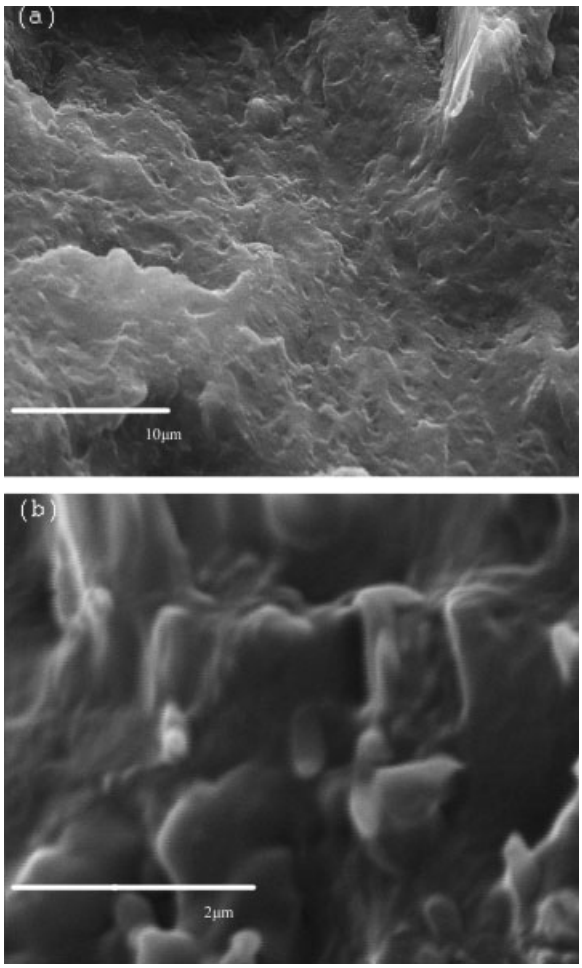


**Figure 7** SEM photomicrographs of cryofractured surfaces of the TPV nanocomposite containing 12 wt % of ME (3 wt % EG). (a) low magnification, (b) high magnification.

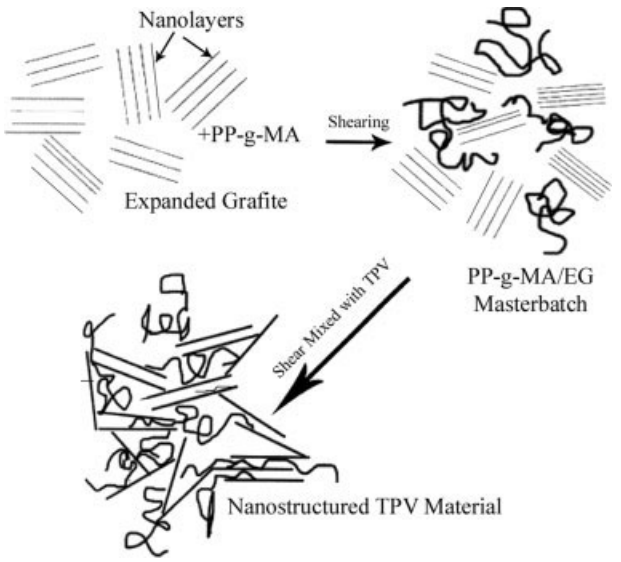


**Figure 8** Model showing the morphology development during melt mixing of *g*-PP/EG masterbatch (ME) and Santoprene TPV.

composed of layered nanofiller is related to the aspect ratio of the filler particles and the mesoscopic network structure formed by the delaminated nanolayers. Therefore, to further study the microstructure of the prepared TPV/graphite nanocomposites, the extent of frequency dependency of the melt viscosity and storage modulus ($G'$) of the samples was investigated and compared. For this purpose, the linear viscoelastic region was first determined for each molten sample by dynamic strain sweep at 220°C, followed by frequency sweep measurements. The strain sweep results for the neat TPV and its corresponding composites based on masterbatches of pp-*g*-MA and NGF, GIC, and EG have been presented and compared in Figure 9(a–d). It is clearly seen that TPV/pp-g-MA/EG nanocomposite sample exhibits shear thinning and non-Newtonian behavior above 1% strain amplitude, while the neat melt processed TPV and TPV composites composed of natural graphite (NGF) as well as intercalated graphite (GIC) retain their linear and Newtonian characteristics up to 10% strain. This indicates the formation of multiple brittle networks by the graphite nanolayers in the matrix of TPV for the TPV/pp-*g*-MA/EG samples, which evidences more exfoliation and dispersion of the graphite nanolayers in this sample. More strain dependency of the melt viscoelastic parameters have also been reported for the TPO/clay nanocomposites with intercalated/foliated morphology compared to their pristine TPO.[34] The melt storage modulus ($G'$) from dynamic frequency scan at 220°C and strain amplitude of 0.5 for unfilled melt processed TPV and its corresponding graphite composite samples are also presented in Figure 10(a–d). It is

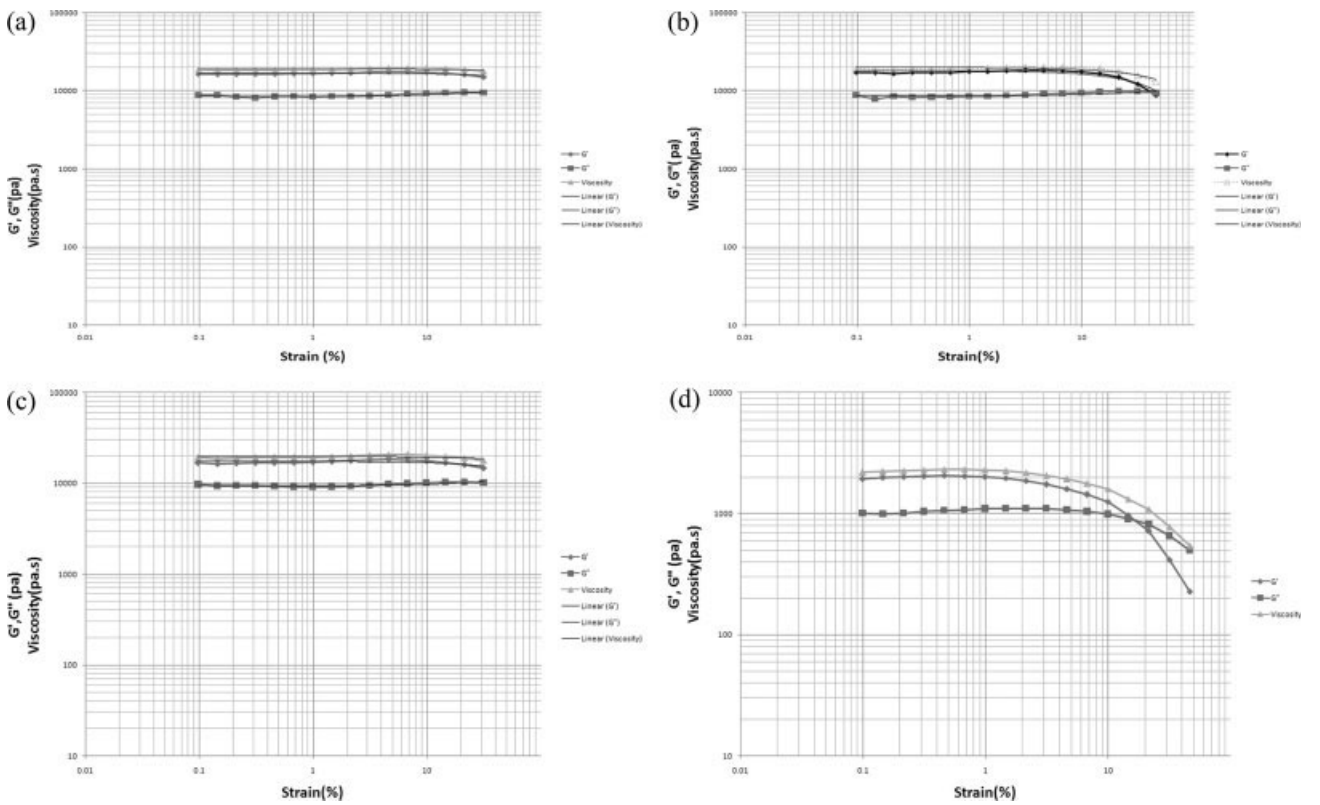


**Figure 9** Dynamic Strain Sweep at the frequency of 1 rad/s and temperature 220°C for: (a) Neat melt processed TPV, (b) TPV/MN, (c) TPV/MGIC, (d) TPV/ME, composites containing 3 wt % of NGF, GIC, EG, respectively.

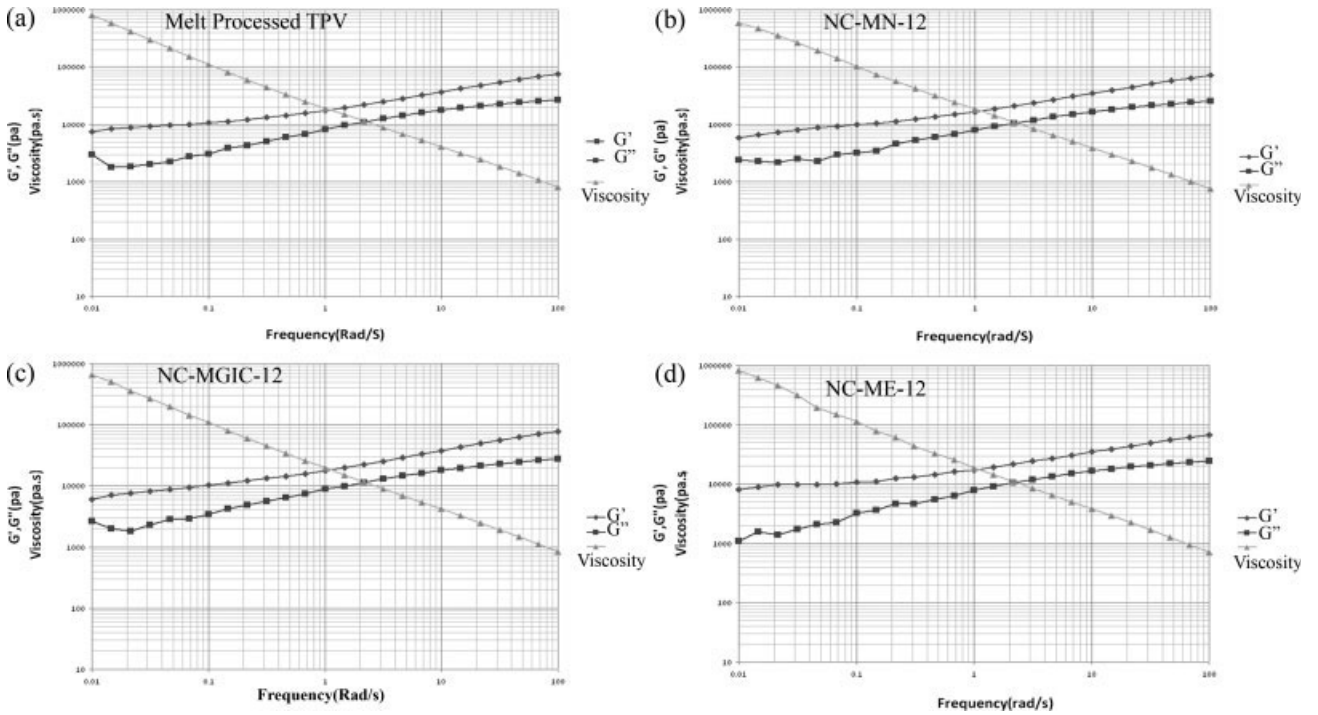


**Figure 10** Linear melt viscoelastic properties at 220°C for (a) Neat meltprocessed TPV, (b) TPV/MN, (c) TPV/MGIC, (d) TPV/ME, composites containing 3 wt % of NFG, GIC, EG, respectively.

obviously observed that the $G'$ of TPV nanocomposite based on exfoliated graphite (EG) show higher magnitude at low frequency with plateau and nonterminal behavior, while the $G'$ of the TPV/pp-*g*-MA/NFG and TPV/pp-*g*-MA/GIC increase monotonically at low frequency with higher slope at high frequency region. These observations indicate the formation of percolated network structure in the TPV/pp-g-MA/EG nanocomposite structure, leading to the solid- like viscoelastic response at low frequency which is attributed to the presence of randomly oriented graphite nanolayers with high aspect ratio within the TPV matrix. The TPV composite sample related to the untreated natural graphite shows lower $G'$ at low frequency due to the lubrication effect of natural graphite, and insignificant interaction between the nonreactive NGF layers with the TPV/PP-*g*-MAH matrix. This evidences weak possibility for the formation of mesoscopic conductive network structure by the NGF nanolayers, and therefore their poor dispersion through out the TPV matrix. It is obvious that in all samples viscous modulus ($G''$) keeps increasing with frequency as a result of time retardation for the matrix to respond to the applied dynamic stress.

## Electrical conductivity

Figure 11, illustrates the volume conductivity (σ) as a function of graphite content for different prepared composites. It is obviously seen that all composites display distinct percolation thresholds ($\varphi_c$), but with different conductivity-graphite content dependency. The TPV/ME nanocomposite samples exhibit a percolation threshold at 6 phr (parts per hundreds resin) of EG, whereas the composites prepared by the melt mixing of TPV and EG in the absence of compatibilizer, show little changes in conductivity up to the 10 wt % of EG. Moreover, TPV/PP-*g*-MA/EG nanocomposite composed of 15 wt % of EG exhibits conductivity order of eight order of magnitude higher than the TPV/EG counterpart. This indi-

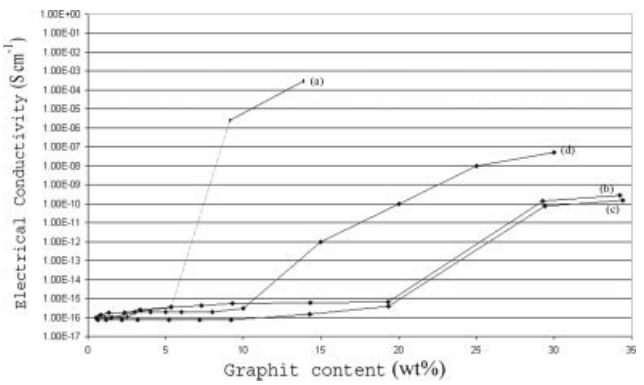


**Figure 11** Variation of electrical conductivity (σ) as a function of graphite content for TPV/graphite composites prepared by melt mixing of santoprene TPV with masterbatches of PP-*g*-MAH (PB) and, (a) Expanded graphite (EG), (b) Natural graphite (NFG), (c) Graphite intercalated compound (GIC), and compared with uncompatibilized TPV/EG composite (d).

cates the formation of infinite continuous conductive networks throughout the TPV matrix in the microstructure of TPV/*g*-PP/EG nanocomposite, implying better dispersion of the EG nanolayers with higher aspect ratio as a result of enhanced interaction between the compatibilized TPV matrix and functional groups existing on the surface of EG. These results show the important role of *g*-pp as interfacial compatibilizer to facilitate delamination of the EG nanolayers, and hence formation of interconnected conductive networks.

Comparing the electrical conductivity for the four composite samples based on graphites with different microstructure, indicates that EG has much higher potentiality to reduce the conductivity percolation threshold than GIC graphite. This could be attributed to the foliated multiporous structure of EG graphite, as well as enhanced interaction of the highly functionalized EG nanolayers with the compatibilized TPV matrix during shear melt mixing process.

## CONCLUSION

Electrically conductive nanocomposite thermoplastic elastomer was fabricated by dispersing nanosheets of EG through out the matrix of the TPV via melt mixing in the presence of maleic anhydride grafted polypropylene (PP-*g*-MA) as interfacial compatibilizer. Percolation threshold ($\varphi_c$) was found to be much lower when EG was compounded with TPV in the form of masterbatch with PP-*g*-MA. TPV/PP-*g*-MA/EG nanocomposites showed electrical conductivity ($\sigma$) eight orders of magnitude higher than that of TPV/PP-*g*-MA/NGF sample, and much lower percolation threshold. This evidences the crucial role of interfacial compatibilizer in enhancing the interaction between the TPV matrix and active functional groups existing on the surfaces of EG, leading to the more foliation of the graphite nanolayers. However, compatibilizer could not be effective in separating the nanolayers in the structure of untreated natural graphite when being melt mixed with TPV. TPV/PP-*g*-MA/EG nanocomposites exhibited more melt shear thinning behavior, and solid like viscoelastic response at low frequency when subjected to a dynamic shear field. XRD, SEM, TEM, and melt dynamic characteristics confirmed that a multiple network structure is formed in the internal structure of TPV/*g*-MAH/EG nanocomposite, which in great improvement of electrical conductivity of the TPV matrix.

The authors gratefully acknowledge the Department of Chemical Engineering of McMaster University of Canada for providing the required materials and instruments. The authors also thank Dr. Michael Thomson from Chemical Engineering Department of McMaster University for providing the PP-g-MA and mixing facilities. Special thanks to the Amirkabir University of Technology of Iran for financially supporting A.A. Katbab to stay on sabbatical leave in Canada.

## References

1. Wang, S.; Hu, Y.; Zhongkai, Q.; Wang, Z.; Chen, Z.; Fan, W. Mater Lett 2003, 57, 2675.
2. Kojima, Y.; Usuki, A.; Kawasumi, Y.; Okada, A.; Kurauchi, T.; Kamigaito, O. J Polym Sci Part A: Polym Chem 1993, 31, 983.
3. Giannelis, E. P. Adv Mater 1996, 8, 29.
4. Oya, A.; Kurokawa, Y. J Mater Sci 2000, 35, 1045.
5. Pinnavaia, T. J.; Beall, G. W., Eds. Polymer Clay Nanocomposites; Wiley: New York, 2001.
6. Vaia, R. A.; Teukolsky, R. K.; Giannelies, E. P. Chem Mater 1994, 6, 1017.
7. Fan, S.; Chapline, M. G.; Franklin, N. R.; Tombler, T. W.; Cassell, A. M.; Dai, H. Science 1999, 283, 512.
8. Sun, J.-S.; Gokturk, H. S.; Malyon, D. M. J Mater Sci 1993, 28, 364.
9. Nagata, K.; Iwabuki, H.; Nigo, H. Comp Interface 1999, 6, 483.
10. Chen, L.; Wong, S. C. J Appl Polym Sci 2003, 88, 3248.
11. Bioteux, G.; Fournier, J.; Issotier, D.; Seytrei, G.; Marichy, G. Synth Met 1999, 102, 1234.
12. Aharoni, S. M. J Appl Phys 1972, 43, 2463.
13. Gabriel, P.; Cipriano, L. G.; Ana, J. M. Polym Comp 1999, 20, 804.
14. Cao, N. Z.; Shen, W. C.; Wen, S. Z.; Liu, Y. J.; Wang, Z. D.; Inagaki, M. J Mater Sci (Chinese) 1996, 14, 22.
15. Semko, L. S.; PoPoV, R. E.; Chernysh, I. G. Int Polym Sci Technol 1997, 24, 71.
16. Wu, G.; Asai, S.; Sumita, M. Macromolecules 1999, 32, 3534.
17. Amunya, E. P. M.; Davidenko, V. V.; Lebedov, E. V. Compos Int 1997, 4, 16.
18. Xiao, P.; Xiao, M.; Gong, K. C. Polymer 2001, 42, 4813.
19. Mallette, J. G.; Marquez, A.; Mnero, O.; Castro-Rodriguez, R. Polym Eng Sci 2000, 40, 2272.
20. King, J. A.; Tucker, K. W.; Vogt, B. D.; Weber, E. H.; Quan, C. L. Polym Compos 1999, 20, 643.
21. Shioyama, H. Synth Met 2000, 114, 1.
22. Par, Y. X.; Yu, Z. Z.; Ou, Y. C.; Hu, G. H. J Polym Sci Part B: Polym Phys 2000, 38, 1626.
23. Xiao, P.; Xiao, M.; Gong, K. C. Polymer 2001, 42, 4813.
24. Chen, G.; Weng, W.; Wu, D. Chen, J.; Ye, L.; Yan, W. Acta Polym Sin 2001, 19, 803.
25. Yi, S. X.; Song, H. Y.; Zhen, Q. J Appl Polym Sci 2000, 77, 792.
26. Kotov, N. A.; Dekany, I.; Fendler, J. H. Adv Mater 1996, 8, 637.
27. Chen, G. H.; Wu, D. J.; Weng, W. G.; Yan, L. W. J Appl Polym Sci 2001, 82, 2506.
28. Shen, J. W.; Huang, W. Y.; Wu, S.; Hou, J. J Appl Polym Sci 2005, 97, 51.
29. Katbab, A. A.; Goharpey, F.; Nazokdast, H. Rubber Chem Technol 2004, 77, 16.
30. Coran, A. Y.; Patel, R. Rubber Chem Technol 1980, 53, 141.
31. Cao, N.; Shen, W.; Wenand, S.; Liu, Y. Chem Bull 1996, 4, 37.
32. Toyoda, M.; Aizawa, J.; Inagaki, M. Desalination 1998, 115, 19.
33. Wang, Y.; Chen, F.-B.; Wu, K.-C.; Wang, J.-C. Polym Eng Sci 2006, 46, 289.
34. Mishra, J.; Hwang, K.; Ha, C.-S. J Polym 2005, 46, 1995.